

A Study of the Branching Ratio of $H \rightarrow c\bar{c}$ at a Future e^+e^- Linear Collider

Yu, Geum Bong* and Kang, JooSang
Department of Physics, Korea University, Seoul, Korea, 136-701

Miyamoto, Akiya
KEK, 1-1 Oho, Tsukuba-Shi, Ibaraki-Ken, Japan, 305-0801

Park, Hwanbae†
Department of Physics, Kyungpook National University, Taegu, Korea, 702-701
(Dated: October 29, 2018)

We carried out a feasibility study on the measurement of the branching ratio of $H \rightarrow c\bar{c}$ at a future e^+e^- linear collider. We used topological vertex reconstruction algorithm for accumulating secondary vertex information and neural network for optimizing c quark selection. With an assumption of a Higgs mass of 120 GeV/ c^2 we estimated statistical uncertainty of $\text{Br}(H \rightarrow c\bar{c})$ to be 20.1% or 25.7% , depending on the number of vertex detector layers, at the center-of-mass energy of 250 GeV and the integrated luminosity of 500 fb $^{-1}$.

PACS numbers: 11.15.Ex, 11.30.Qc, 14.65.Dw, 14.80.Bn

I. INTRODUCTION

In the theory of elementary particles, Higgs boson is introduced to elucidate the origin of particle masses. The Standard Model (SM) proposed the single Higgs doublet that gives rise to a scalar particle, while extended supersymmetric models hypothesized that two Higgs doublets give separate vacuum expectation values to the up-type and down-type quarks. Among the extended models beyond SM, the Minimal Supersymmetric Standard Model (MSSM) sets the upper bound of the lightest neutral Higgs mass around 130 GeV/ c^2 [1]. Since the mass of SM Higgs boson is expected to be between 114.4 GeV/ c^2 and 211 GeV/ c^2 by LEP experiment[2], the Higgs boson should be identified if it is found. Therefore a precise measurement of Higgs couplings to fermions at a future e^+e^- linear collider is indispensable to unveil physics of the Higgs sector. In particular, a measurement of the branching ratio of $H \rightarrow c\bar{c}$ would provide a unique opportunity to study Higgs to up-type quark coupling. However, the $H \rightarrow b\bar{b}$ is the dominant process for Higgs mass below 140 GeV/ c^2 .

A high efficient charm quark identification is necessary for the precise branching ratio study and it is possible only with a high performance vertex detector. Development of this vertex detector has been a major issue for the linear collider [3]. To this end, understanding detector performance is extremely important to physics.

In this paper, we introduce our method of measuring the branching ratio of $H \rightarrow c\bar{c}$ against SM e^+e^- processes and other decay branches from Higgs. In addition, we

would like to see the significance of this precision study with four layers of Charge Coupled Device (CCD) and an additional inner layer of vertex detector.

II. HIGGS SIMULATION

A mass of SM Higgs boson is assumed to be 120 GeV/ c^2 and the center-of-mass energy of 250 GeV is selected by the highest s -channel production cross-section at this energy, 226 fb. It is concerned with an integrated luminosity of 500 fb $^{-1}$ for the first few years running of the future e^+e^- linear collider experiment.

Events were generated using PYTHIA 5.7 [4] and only the Higgsstrahlung process ($e^+e^- \rightarrow Z^* \rightarrow Z^0 H$) was taken into account. The branching ratios of the SM Higgs boson was estimated by the HDecay program [5]. Depending on the decay modes of Z^0 , the events are categorized into 4-jet mode ($Z^0 \rightarrow q\bar{q}$ and $H \rightarrow q\bar{q}$), 2-jet mode ($Z^0 \rightarrow \nu\bar{\nu}$ and $H \rightarrow q\bar{q}$), and charged lepton pair mode ($Z^0 \rightarrow \ell^+\ell^-$ and $H \rightarrow q\bar{q}$). Since the branching ratio of Higgs to $c\bar{c}$ is estimated to be very small ($\sim 3\%$), we concentrated on the 2-jet and 4-jet modes only. As background processes from e^+e^- collision, W^+W^- , Z^0Z^0 , and $q\bar{q}$ events were considered with corresponding cross-sections of 15460 fb, 1250 fb, and 47300 fb, respectively.

The detector simulation was performed using a fast parameterized simulator [6], which is implemented in the Joint Linear Collider (currently called as Global Linear Collider) detector [7]. In this simulator five parameters of the helical track and their error matrices including non-diagonal elements were generated; thus the quality of the vertices is similar to that of a full simulation. The JLC vertex detector is equipped with four layers of CCD at the radius from 2.4 cm to 6 cm of which intrinsic spatial resolutions are 4 μm in $r\phi$ and z directions. The solenoidal magnet field of the detector is 3 tesla. With

*Current address: Department of Physics and Astronomy, University of Rochester, Rochester, NY 14627, U.S.A.

†Corresponding author: sunshine@knu.ac.kr

number of CCD layers	Beam pipe	1st	2nd	3rd	4th	5th
4	2.0	2.4	3.6	4.8	6.0	
5	1.0	1.2	2.4	3.6	4.8	6.0

TABLE I: Two vertex detector parameter set. the number of CCD layers and their positions(in cm) from the center of the beam pipe, the radius of beam pipe are listed for each set.

a vertex detector constraint, the impact parameter resolution in xy plane ($\sigma_{r\phi}$) is $\sqrt{(25/p\sin^2/3\theta)^2 + 4^2}$ μm , and the momentum resolution for charged track ($\Delta p_t/p_t$) is $\sqrt{(1 \times 10^{-4} p_t)^2 + 10^{-3}}$. This study was done with four/five CCD layers of vertex detector parameter, respectively, to see the influence of the vertex detector options on the physics result. The vertex detector parameter sets are shown in the Table I.

In the event reconstruction, jets were reconstructed using JADE clustering algorithm [8] and the vertices were reconstructed using the topological vertex reconstruction algorithm (ZVTOP program) [9]. Based on kinematic variables and reconstructed vertex information, an artificial neural network (NN) [10] is formed to identify $H \rightarrow c\bar{c}$ events more efficiently.

We considered the non- $c\bar{c}$ Higgs decays ($H \rightarrow b\bar{b}$, gg , WW^* ; Higgs background) and other processes from e^+e^- collision ($e^+e^- \rightarrow Z^0Z^0$, W^+W^- , $q\bar{q}$; non-Higgs background) as backgrounds of $H \rightarrow c\bar{c}$ measurement.

III. SELECTION OF $H \rightarrow c\bar{c}$

A. 2-jet mode

In 2-jet mode all clustered particles are forced to make 2 jets by adjusting the maximum value of y_{cut} [13], Y_{max} . The following selections are applied to reduce non-Higgs background in the sample: (1)visible energy between 110 GeV and 143 GeV, (2)missing transverse momentum between 25 GeV/ c and 70 GeV/ c , (3)Higgs mass between 105 GeV/ c^2 and 125 GeV/ c^2 , (4)recoiled Z^0 mass between 82 GeV/ c^2 and 120 GeV/ c^2 , (5)thrust between 0.75 and 0.99, (6) Y_{max} between 0.72 and 0.84, and (7)mass of each jet between 2 GeV/ c^2 and 40 GeV/ c^2 . Here the Higgs mass is an invariant mass of all the observed particles and the recoiled Z^0 mass is calculated disregarding the initial state radiation. We also require a successful secondary vertex reconstruction and at least one P_t corrected invariant mass (MSPTM, $\sqrt{M^2_{\text{VTX}} + P_t^2 + |P_t|}$) of the secondary vertex to be between 0.1 GeV/ c^2 and 7.0 GeV/ c^2 , where P_t is the total transverse momentum of the secondary tracks with respect to the flight direction of the vertex. The separation between signal and non-Higgs background is clearly seen in Fig. 1, while Higgs background is not distinguishable in this aspect.

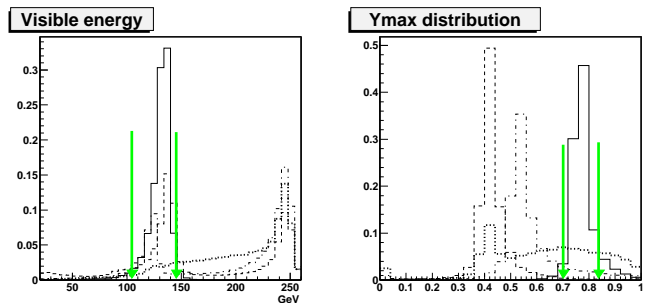


FIG. 1: Visible energy and Y_{max} distributions in 2-jet mode are shown. Arrows are place on the cut value. Solid: Z^0H , dotted: W^+W^- , dash-dotted: Z^0Z^0 , dashed: $q\bar{q}$.

After the sample selection, NN is trained to maximize the selection quality. Two sets of training are used; one against non-Higgs backgrounds (Background NN-training) and the other against Higgs backgrounds (Higgs NN-training). For each NN-training $H \rightarrow WW^*$ and $e^+e^- \rightarrow q\bar{q}$ processes are not used due to the featureless patterns and small statistics, respectively.

The normalized input patterns for NN-trainings were given from the ZVTOP program; the number of vertices, MSPTM, transverse momentum of the secondary vertex, decay length, invariant mass of the secondary vertex, number of tracks in the secondary vertex, and momentum of the secondary vertex divided by total momentum (corrected secondary momentum). Distinctive input patterns for Higgs NN-training and Background NN-training are shown in Fig. 2 and Fig. 3, respectively. In the Background NN-training Y_{max} and jet decay angle were included in the input patterns especially for this 2-jet mode.

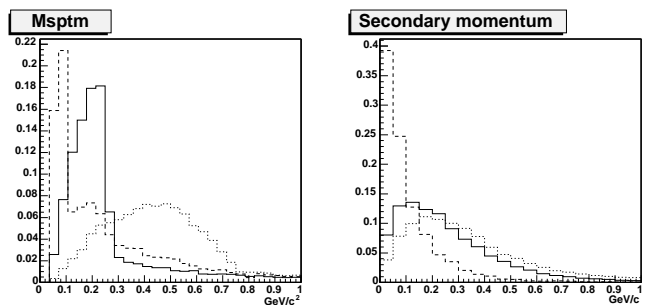


FIG. 2: MSPTM and the corrected secondary momentum distributions are used as input patterns for $H \rightarrow c\bar{c}$ distinction from Higgs backgrounds in 2-jet mode. Solid: $H \rightarrow c\bar{c}$, dotted: $b\bar{b}$, dashed: gg .

Using both results of Higgs NN-training and Background NN-training, the signal region is evaluated in two dimensional plane for best significance. The signal selection area is shown in the top right corner of the Fig. 4.

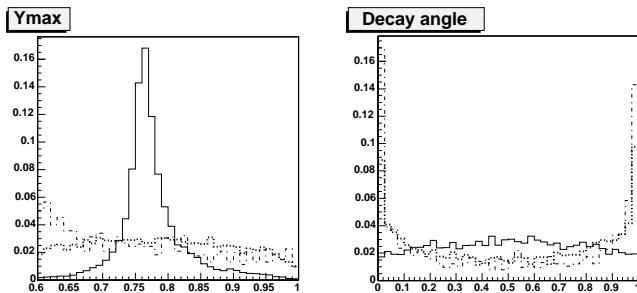


FIG. 3: Ymax and decay angle distributions show good separation between $c\bar{c}$ and non-Higgs backgrounds in 2-jet mode. They are used as input patterns for Background NN-training. Solid: $Z^\circ H$, dotted: W^+W^- , dash-dotted: $Z^\circ Z^\circ$.

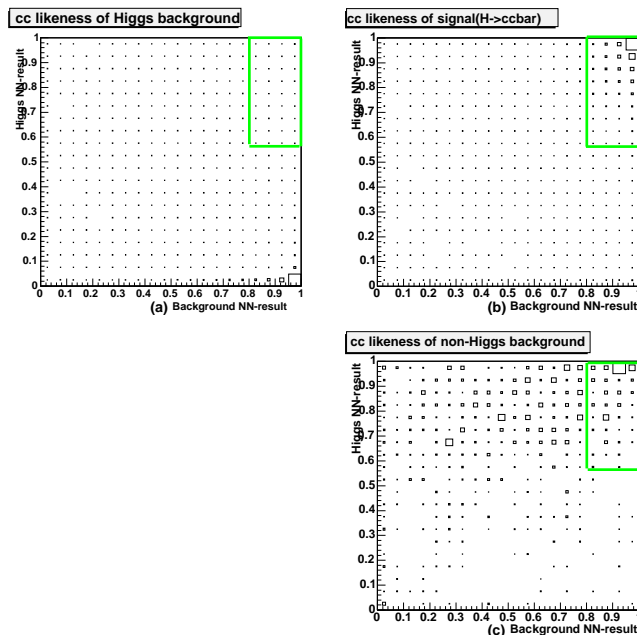


FIG. 4: 2D NN-result for $H \rightarrow c\bar{c}$ selection in 2-jet mode; (a) Higgs backgrounds, (b) $H \rightarrow c\bar{c}$ signal event, and (c) non-Higgs backgrounds. The signal region is seen at the top right.

B. 4-jet mode

Here we used forced 4-jet clustering for Higgs jet pair and Z° jet pair. The jets are identified by minimum χ^2 , which is defined as the squared sum of the differences between reconstructed invariant mass of jet pair and the expected mass divided by each mass resolution:

$$\chi^2 = \left(\frac{M_{Z^\circ} - 91.2}{\text{width}}\right)^2 + \left(\frac{M_{\text{recoil}Z^\circ} - 91.2}{\text{width}}\right)^2 + \left(\frac{M_H - 120}{\text{width}}\right)^2 + \left(\frac{M_{\text{recoil}H} - 120}{\text{width}}\right)^2.$$

The selection cuts were made: (1) visible energy greater than 210 GeV, (2) $\cos\theta$ of thrust axis (thrust angle) between -0.85 and 0.85 , (3) Higgs mass between

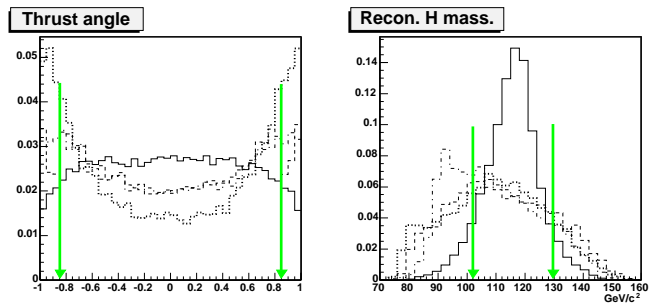


FIG. 5: Thrust angle and Higgs mass distributions in 4-jet mode are shown. Arrows are placed on the cut value. Solid: $Z^\circ H$, dotted: W^+W^- , dash-dotted: $Z^\circ Z^\circ$, dashed: $q\bar{q}$.

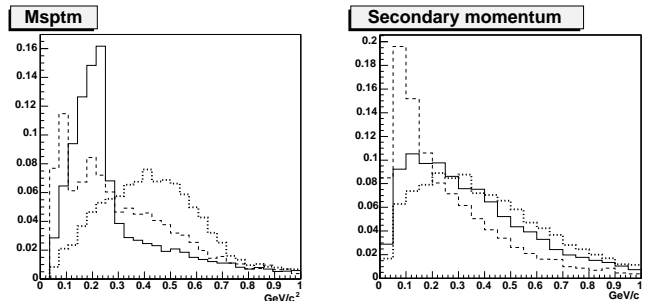


FIG. 6: MSPTM and the corrected secondary momentum distributions in 4-jet mode. They are used for $H \rightarrow c\bar{c}$ distinction from non- $c\bar{c}$ Higgs decays in Higgs NN-training. Solid: $H \rightarrow c\bar{c}$, dotted: $b\bar{b}$, dashed: $g\bar{g}$.

103 GeV/c^2 and 130 GeV/c^2 , (4) Z° mass between 78 GeV/c^2 and 102 GeV/c^2 , (5) mass recoiled to the Higgs jet pair greater than 80 GeV/c^2 , (6) number of particles in each jet of Higgs pair greater than 5, and (7) Ymax value greater than 0.01.

Only 2 jets which are assigned to Higgs are used for the vertex tagging. We also required at least one successful secondary vertex reconstruction with MSPTM between 0.1 GeV/c^2 and 7.0 GeV/c^2 out of 2 jets from Higgs. The distributions of Higgs mass and thrust angle are shown in the Fig. 5. With the same procedure as the 2-jet study, we trained the NN against non-Higgs background and Higgs background separately using normalized vertex information from the ZVTOP program. The MSPTM and the corrected secondary momentum distributions of the $c\bar{c}$ and the non- $c\bar{c}$ Higgs decays are seen in the Fig. 6. We did not use $H \rightarrow WW^*$ events in Higgs NN-training due to their featureless patterns. In the Background NN-training, thrust angle is added in the input pattern. As seen in the Fig. 7, the thrust angle shows a clear separation between the signal and non-Higgs backgrounds. We use both results of Higgs NN-training and Background NN-training same as 2-jet mode. The 2D NN-results are shown in the Fig. 8 with signal box at the top right.

Number of CCD layers	4 CCD layers		5 CCD layers	
Decay mode \ Events	2-jet	4-jet	2-jet	4-jet
$H \rightarrow c\bar{c}$	122.7(17.6)	306.3(12.6)	112.7(16.2)	316.8(13.0)
$H \rightarrow b\bar{b}$	641.8(4.2)	2686.7(5.0)	231.2(1.5)	1807.2(3.4)
$H \rightarrow gg$	28.1(1.8)	217.6(3.9)	8.9(0.6)	143.4(2.6)
$H \rightarrow WW^*$	23.6(0.8)	226.7(2.1)	10.1(0.3)	178.0(1.7)
$e^+e^- \rightarrow W^+W^-$	640(0.008)	9790(0.130)	330(0.004)	8530(0.110)
$e^+e^- \rightarrow Z^0Z^0$	100(0.016)	1710(0.274)	30(0.004)	1305(0.209)
$e^+e^- \rightarrow q\bar{q}$	20(<0.001)	1730(0.007)	5(<0.001)	1345(0.006)
S/N	0.0843	0.0187	0.1832	0.0238
$S/\sqrt{S+N}$	3.09	2.37	4.17	2.71
Statistical uncertainty		25.7 %		20.1 %

TABLE II: The number of c quark tagged events, efficiency (percentage in parenthesis), and significance (last three rows) of $H \rightarrow c\bar{c}$ measurements for two different vertex detector parameters. The statistical uncertainty (last row) is calculated combining significance of 2-jet and 4-jet. We used 100 fb^{-1} in this analysis and scaled up to 500 fb^{-1} in this table.

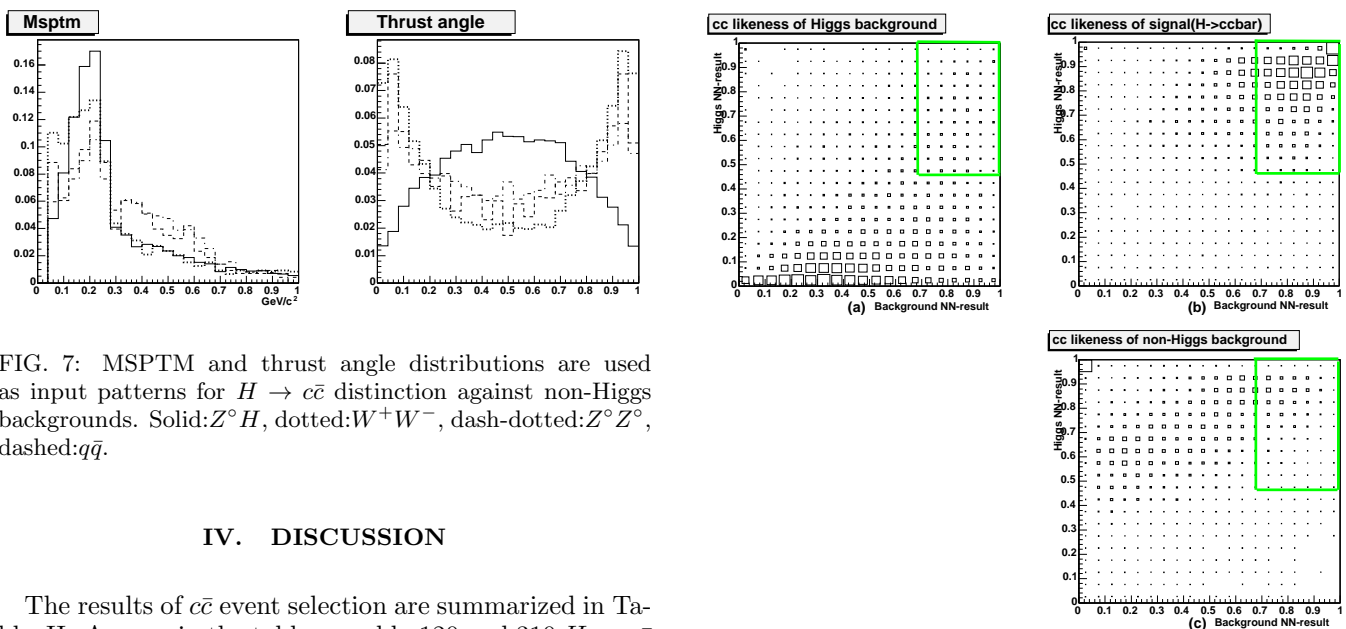


FIG. 7: MSPTM and thrust angle distributions are used as input patterns for $H \rightarrow c\bar{c}$ distinction against non-Higgs backgrounds. Solid: $Z^0 H$, dotted: W^+W^- , dash-dotted: $Z^0 Z^0$, dashed: $q\bar{q}$.

IV. DISCUSSION

The results of $c\bar{c}$ event selection are summarized in Table II. As seen in the table, roughly 120 and 310 $H \rightarrow c\bar{c}$ events are selected in 2-jet and 4-jet modes, respectively, with a reasonable significance despite its small branching ratio of $H \rightarrow c\bar{c}$ and large backgrounds from non-Higgs processes and non- $c\bar{c}$ Higgs decays.

In the $H \rightarrow c\bar{c}$ measurement in 2-jet mode, major backgrounds are those from $H \rightarrow b\bar{b}$ where b is misidentified as c and W^+W^- events which are reconstructed as 2-jet events due to imperfect detector acceptance. $e^+e^- \rightarrow \nu W$ is not considered here due to relatively small cross-section than other background processes.

In the case of 4-jet mode, W^+W^- and Z^0Z^0 events are increased after event selection because two c jets can be produced in the final state of these processes. In addition to the c-jet contamination from backgrounds, there is additional ambiguity in selecting two Higgs jets out of four jets. Combining these effects, the significance in the 4-jet mode is less than 3σ and worse than the 2-jet mode. The statistical uncertainty combining 2-jet and 4-jet analyses is estimated as 25.7% in the case of four CCD layers of the vertex detector. Similar analysis

FIG. 8: 2D NN-results for $H \rightarrow c\bar{c}$ selection in the 4-jet mode; (a)Higgs backgrounds, (b) $H \rightarrow c\bar{c}$ signal event, and (c)non-Higgs backgrounds. The signal region is seen at the top right.

with different detector configuration was report[12] for assumption of the same Higgs mass and luminosity at $\sqrt{s}=350 \text{ GeV}$ and 500 GeV that the relative branching ratio errors be 19% and 39%, respectively.

When an additional CCD layer of the vertex detector is included near the interaction point, the impact parameter resolution for low momentum track is improved since the lever arm for track extrapolation to the interaction point is reduced. Thus we can reconstruct secondary vertices much closer to the interaction point. The better separation of b - and c - jets reduces backgrounds in the event selection, especially in 2-jet mode. Improvements in 4-jet selection is not decisive, suffering ambiguities in Higgs jet selections. Combining 2-jet and 4-jet,

relatively 20% improvement in background reduction is achieved compared to the study with four CCD layers of the vertex detector.

V. SUMMARY

In this study we focused on the $H \rightarrow c\bar{c}$ measurements in 2-jet and 4-jet modes in the case of 120 GeV/ c^2 Higgs mass at the center-of-mass energy of 250 GeV in the future e^+e^- linear collider. In the study, the topological vertex finding algorithm was used for tagging the c -jet and the neural network was used to optimize the $H \rightarrow c\bar{c}$ selection.

With consideration of 500 fb $^{-1}$ data, we obtained the statistical uncertainty of 25.7% for the measurement of $H \rightarrow c\bar{c}$ with four CCD layers vertex detector. The sta-

tistical uncertainty would be improved to 20.1% with an additional CCD layer of vertex detector near the interaction point.

VI. ACKNOWLEDGMENT

We would like to thank the members of ACFA Joint Linear Collider Physics and Detector Working group [11] for valuable discussions during the course of the analysis. We also thank Dr. David Jackson for allowing us to use his ZVTOP program. We acknowledge the support by Korea Research Foundation Grant funded by Korea Government (MOEHRD) (KRF-2005-070-C000321) and Korea Science and Engineering Foundation. Akiya Miyamoto is partially supported by Japan-Europe Research Cooperative Program.

-
- [1] J. Kamoshita, Y. Okada, and M. Tanaka, Phys. Lett. **328B**, 67 (1994) ; T. Moroi and Y. Okada, Phys. Lett. **295B**, 73 (1992).
 - [2] The LEP Collaborations, the LEP Electroweak Working Group, and the SLAC heavy flavour group, LEPEWWG/2003-01 (2003).
 - [3] “Report on the international detector R & D”, See “<http://blueox.uoregon.edu/~lc/randd.html>”.
 - [4] T. Sjostrand, Comput. Phys. Commun. **82**, 74 (1994).
 - [5] A. Djouadi, J. Kalinowski, and M. Spira, Comput. Phys. Commun. **108**, 56 (1998).
 - [6] JLC Study Framework, See “<http://www-jlc.kek.jp/subg/offl/jsf>”.
 - [7] K. Abe *et al.*, KEK Report 2001-11 (2001).
 - [8] JADE Collaboration, Phys. Lett. **213B**, 235 (1988)
 - [9] D. J. Jackson, Nucl. Instrum. Meth. **A 388**, 247 (1997).
 - [10] C. Peterson, T. Rognvaldsson, and L. Lonnblad, Comput. Phys. Commun. **81**, 185 (1994).
 - [11] See “<http://acfahep.kek.jp>”.
 - [12] C.T. Potter, J.E. Brau and N.B. Sinev, Nucl. Instrum. Meth. **A 511**, 225 (2003).
 - [13] $y_{ij} = \frac{2E_i E_j (1 - \cos\theta_{ij})}{E_{\text{visible}}^2}$, where E_i and E_j are energy of i -th and j -th cluster, respectively, and θ_{ij} is angle between two clusters.